



CHORUS

This is the accepted manuscript made available via CHORUS. The article has been published as:

Magnetic Nanoantennas Made of Plasmonic Nanoclusters for Photoinduced Magnetic Field Enhancement

Mahsa Darvishzadeh-Varcheie, Caner Guclu, and Filippo Capolino

Phys. Rev. Applied **8**, 024033 — Published 31 August 2017

DOI: [10.1103/PhysRevApplied.8.024033](https://doi.org/10.1103/PhysRevApplied.8.024033)

Magnetic Nanoantennas Made of Plasmonic Nanoclusters for Photoinduced Magnetic Field Enhancement

Mahsa Darvishzadeh-Varcheie, Caner Guclu, Filippo Capolino*

Department of Electrical Engineering and Computer Science, University of California, Irvine, CA, 92697, USA

*f.capolino@uci.edu

We focus on a category of nanoantennas called magnetic nanoantennas, made of a circular cluster of gold nanospheres, that leads to enhanced local magnetic field oscillating at optical frequency. We elaborate on the magnetic field enhancement and the magnetic to electric field ratio, i.e., the local field admittance, when the nanoantenna is illuminated by a single plane wave and by superposition of two plane waves to maximize the magnetic-only response. Single dipole approximation (SDA) is used to analyze magnetic nanoantennas and verified by our findings with full wave simulations. We derive a formula that estimates the natural frequency associated to the magnetic resonance of a circular plasmonic cluster with an arbitrary number of plasmonic nanospheres. Lastly, we classify clusters based on their quality factor, their ability to enhance the magnetic field, and discuss the surface area with strong magnetic field provided by the plasmonic cluster.

I. INTRODUCTION

The magnetic interaction of light and matter is weaker than its electric counterpart at optical frequencies [1–4]. Due to this reason, achieving resonant magnetism in the optical regime has become the focus of attention in the physics and engineering communities [5–11]. The overall magnetism of a metamaterial (i.e., relative magnetic permeability different from unity) is tailored by engineering the artificial magnetic resonance in “meta-atoms” [12,13]. For instance, engineered metamaterials with magnetic response was demonstrated in [14–18]. Split ring resonators (SRR) are the most explored building blocks in engineering artificial magnetism at the microwave spectrum [19–22]. Moreover, in [23–26], it is shown that by tuning the dimensions of SRR and by implementing a precise fabrication, the magnetic resonance at near infrared and visible frequencies, is achievable. In [27–30] using effective medium theory, a three-dimensional collection of polaritonic, nonmagnetic spheres have been shown to produce negative permeability at terahertz and infrared frequencies. Furthermore, other structures such as the spherical constellations [31–35], composite medium made of arrays of dielectric spheres [36], a periodic lattice of clusters comprising four silver plasmonic dimers [37] have been used to make metamaterial constituents which provide magnetic polarization in the visible and infrared spectrum.

Circular clusters made of plasmonic nanoparticles, which are of interest in this paper, not only can provide engineered negative permeability [38], but also they can be used to achieve Fano resonances [39–43], and as magnetic nanoprobles enhance light matter interaction [44,45] at optical frequencies.

Conventionally, plasmonic nanoantennas are utilized at optical frequencies owing to their exotic property of enhancing the electric field. However, here we relate to the important quest to enhance magnetic field instead of the electric field [46]. In this paper, inspired by these referenced studies, we focus on the specific category of plasmonic

nanoantennas made of circular clusters and focus on the enhancement of magnetic field. We refer to these antennas as magnetic nanoantennas or magnetic nanoprobles in the rest of the paper. Magnetic nanoantennas can be useful for enhancing quantum magnetic transitions in molecules which are in general overshadowed by the electric ones [47–50,44,45]. The magnetic resonance in a cluster of plasmonic nanoparticles corresponds to a dark resonance, i.e., a resonance that is neither easy to excite nor easy to measure its scattered field, which have higher quality factor and narrower bandwidth than the bright electric resonance counterpart. In [49], a cluster of six silver nanospheres has been studied under azimuthally polarized beam which selectively excites the dark resonance of the cluster with attention to the magnetic field enhancement and to the local field admittance of the scattered near-field. However, to the best of the authors’ knowledge, the exploration of the best clusters for magnetic field enhancement and the amount or surface area where such enhancement occurs is still lacking in the literature as well as a simple analytic formula that estimates the magnetic resonance frequency, given here for the first time.

Hence, in this paper we investigate properties of different clusters of gold nanospheres, such as dimers, trimers, tetramers, pentamers, hexamers, and octamers in a host dielectric medium (e.g., glass or a general solution). Plasmonic gold nanoparticles have applications in medical diagnostics [51,52], sensing [53–56] and imaging [57] in the optical spectrum because of moderately low-loss compared to several other metals and also they are one of the least reactive chemical elements. Our goal is to investigate how magnetic nanoantennas made of gold are able to create a magnetic dominant region in which the magnetic field is enhanced over a certain surface area where the electric field ideally vanishes. Specific figures of merit (the magnetic field enhancement and the normalized local field admittance) are defined and used for that purpose as explained in the next Section.

II. STATEMENT OF THE PROBLEM

We consider clusters of gold nanospheres with various numbers of elements, relative permittivity ϵ_m in a host medium with relative permittivity ϵ_h , shown in Fig. 1. For the purpose of stressing the capabilities of magnetic nanoantennas in boosting quantum magnetic transitions in matter that are overshadowed by electrical ones, we define two figures of merit [49]: the magnetic field enhancement and the magnetic to electric field ratio, i.e. the normalized local field admittance:

$$F_H = \frac{|\mathbf{H}^t(\mathbf{r})|}{|\mathbf{H}^i(\mathbf{r})|} \quad (1)$$

$$F_Y = \eta \frac{|\mathbf{H}^t(\mathbf{r})|}{|\mathbf{E}^t(\mathbf{r})|} \quad (2)$$

Here, $|\mathbf{H}^t(\mathbf{r})|$ and $|\mathbf{E}^t(\mathbf{r})|$ are the magnitude of total magnetic and electric fields at position \mathbf{r} , and $|\mathbf{H}^i(\mathbf{r})|$ is the magnitude of incident magnetic field at the same position, respectively. The magnetic field enhancement (F_H) indicates the ability of a magnetic nanoantenna to enhance the magnetic field with respect to the incident one. The normalized magnetic to electric field ratio, i.e., the normalized local field admittance (F_Y), shows the ability of a magnetic nanoantenna to enhance the magnetic field relatively to the total electric field, normalized to the field impedance $\eta = \sqrt{\mu_0 / (\epsilon_0 \epsilon_h)}$ of a plane wave in the same host medium. Large local admittance in a region shows the magnetic nanoantenna succeeds in generating a magnetic dominant region, and $F_Y > 1$ means that the magnetic to electric field ratio is larger than that of a plane wave.

Scattering from magnetic nanoantennas is characterized using two types of illuminations: (i) a single plane wave, (ii) two counter-propagating plane waves with anti-symmetric electric field with respect to the cluster symmetry plane (y - z plane in Fig. 1) to have a vanishing electric field at the center where a maximum of incident magnetic field occurs. The symmetry of illumination can be further augmented using azimuthally polarized beams with longitudinal magnetic field on their axis [49,58,59] whose field disposition matches perfectly to the magnetic mode of the clusters characterized by the rotationally symmetrical circulating electric dipole moments about the cluster center. The two counter-propagating plane waves excitation is preferred over azimuthally polarized beam illumination solely due to its instant availability and relaxed computation resource requirements in commercial electromagnetic full-wave simulation software packages.

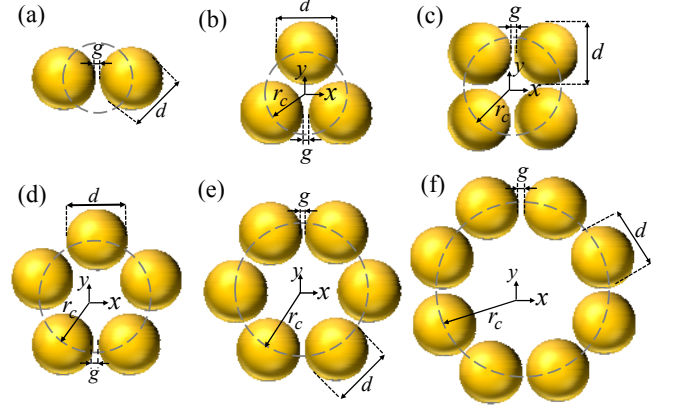


FIG. 1. Plasmonic clusters with varying number of nanospheres: (a) dimer, (b) trimer, (c) tetramer, (d) pentamer, (e) hexamer, and (f) octamer. r_c is the cluster radius and g is the gap between nanoparticles with diameter d .

The cluster types used in our investigation, namely dimers, trimers, tetramers, pentamers, hexamers and octamers are illustrated in Fig. 1. In all structures, the diameter of the nanospheres is “ d ” and the gap between them is “ g ”. For a cluster made of N spheres, each sphere is centered at the corners of a regular polygon whose circumscribed circle has radius r_c called here the cluster radius, given by

$$r_c = \frac{d + g}{2 \sin(\pi/N)} \quad (3)$$

In this paper, the monochromatic time harmonic convention $\exp(-i\omega t)$ is implicitly assumed and the notation is suppressed. In all equations, bold fonts are used for vector quantities in phasor domain, and a bar under a bold font is used for dyadic quantities. Unit vectors are bold with a hat on top.

III. ANALYTIC FORMULATION

We apply the single dipole approximation (SDA) method to model clusters of nanoparticles [60,61]. It means we model each nanosphere with a single electric dipole moment \mathbf{p} . The electric dipole moment of the n^{th} nanosphere at location \mathbf{r}_n is found by

$$\mathbf{p}_n = \alpha \mathbf{E}^{loc}(\mathbf{r}_n) \quad (4)$$

where α is the electric polarizability of the nanosphere, assumed to be isotropic and $\mathbf{E}^{loc}(\mathbf{r}_n)$ is the local electric field at the n^{th} nanosphere’s location which is the summation of the incident field and the field scattered by all the other nanospheres of the cluster. The electric polarizability of the nanospheres is here given by its Clausius-Mossotti expression with the correction term that accounts for the radiation [60]

$$\alpha = \pi \varepsilon_0 \varepsilon_h d^3 \left(2 \frac{\varepsilon_m + 2\varepsilon_h}{\varepsilon_m - \varepsilon_h} - i \frac{(kd)^3}{6} \right)^{-1} \quad (5)$$

where ε_h is the relative permittivity of the host medium, ε_0 is the vacuum permittivity, d is the diameter of the nanosphere, $k = k_0 \sqrt{\varepsilon_h}$ is the host medium wavenumber and k_0 is the wavenumber in vacuum. The gold nanosphere is described by its relative permittivity ε_m given here by the Drude model as

$$\varepsilon_m = \varepsilon_\infty \left[1 - \frac{\omega_p^2}{\omega(\omega + i\gamma)} \right] \quad (6)$$

where ε_∞ is the high-frequency fitting parameter, ω_p is the plasma frequency and γ is the damping factor. For gold, we assume $\varepsilon_\infty = 9.5$, $\omega_p = 4.4124 \times 10^{15}$ rad/s, and $\gamma = 1.05 \times 10^{14}$ rad/s [62].

The total electromagnetic fields at an arbitrary observation point \mathbf{r}_{obs} is given by [63]

$$\mathbf{E}^t(\mathbf{r}_{obs}) = \mathbf{E}^i(\mathbf{r}_{obs}) + \sum_{n=1}^N \underline{\mathbf{G}}(\mathbf{r}_{obs}, \mathbf{r}_n) \cdot \mathbf{p}_n \quad (7)$$

$$\mathbf{H}^t(\mathbf{r}_{obs}) = \mathbf{H}^i(\mathbf{r}_{obs}) + \sum_{n=1}^N \frac{ck^2}{4\pi} \frac{e^{ikr}}{r} \left(1 - \frac{1}{ikr} \right) (\hat{\mathbf{r}}_{obs} \times \mathbf{p}_n) \quad (8)$$

where c is the speed of light in the host medium, and $\underline{\mathbf{G}}(\mathbf{r}_{obs}, \mathbf{r}_n)$ is the dyadic Green's function defined as

$$\underline{\mathbf{G}}(\mathbf{r}_{obs}, \mathbf{r}_n) = \frac{e^{ikr}}{4\pi \varepsilon_0 \varepsilon_h} \left[\left(\frac{k^2}{r} + \frac{ik}{r^2} - \frac{1}{r^3} \right) \mathbf{I} - \left(\frac{k^2}{r} + \frac{3ik}{r^2} - \frac{3}{r^3} \right) \hat{\mathbf{r}} \hat{\mathbf{r}} \right] \quad (9)$$

In Eq. (8) and Eq. (9), $r = |\mathbf{r}|$ with $\mathbf{r} = \mathbf{r}_{obs} - \mathbf{r}_n$, where \mathbf{r}_n is the source dipole location and \mathbf{I} is the 3×3 identity dyad.

The overall electric dipole and overall magnetic dipole moments of a cluster of N nanospheres with the cluster center at the origin are defined as [43]

$$\mathbf{p} = \sum_{n=1}^N \mathbf{p}_n, \quad \mathbf{m} = \frac{-i\omega}{2} \sum_{n=1}^N \mathbf{r}_n \times \mathbf{p}_n \quad (10)$$

respectively.

According to Eq. (7) and Eq. (8), to calculate the electric and magnetic field, the induced electric dipole for each sphere needs to be found. In doing so, we need to construct and solve a linear system of equations in terms of the induced dipole moments and the external excitation field. The local electric field $\mathbf{E}^{loc}(\mathbf{r}_n)$, is given by

$$\mathbf{E}^{loc}(\mathbf{r}_n) = \mathbf{E}^i(\mathbf{r}_n) + \sum_{\substack{m=1 \\ m \neq n}}^N \underline{\mathbf{G}}(\mathbf{r}_n, \mathbf{r}_m) \cdot \mathbf{p}(\mathbf{r}_m) \quad (11)$$

By writing Eq. (4) and Eq. (11) for $n=1, \dots, N$, we can construct the linear system

$$[A] \begin{bmatrix} \mathbf{p}_1 \\ \vdots \\ \mathbf{p}_N \end{bmatrix} = \begin{bmatrix} \alpha \mathbf{E}^i(\mathbf{r}_1) \\ \vdots \\ \alpha \mathbf{E}^i(\mathbf{r}_N) \end{bmatrix} \quad (12)$$

where $[A]$ is a $3N \times 3N$ matrix made of 3×3 sub-blocks $\underline{\mathbf{A}}_{nm}$, with $n, m \in \{1, \dots, N\}$, given by

$$\underline{\mathbf{A}}_{nm} = \begin{cases} \mathbf{I} & m = n \\ -\alpha \underline{\mathbf{G}}(\mathbf{r}_n, \mathbf{r}_m) & m \neq n \end{cases} \quad (13)$$

As mentioned earlier, one of the goals of this paper, is to sort the magnetic nanoantennas based on their quality factor associated to the magnetic resonance, that depends on both material and radiation losses that are accounted for by using the dynamic Green's function (Eq.(9)). One way to calculate the quality factor of each cluster, is to find the cluster natural frequencies. To do so, we need to solve Eq. (12) for ω when $\mathbf{E}_i = 0$. One has non-trivial solutions to such a system only when

$$\det[\underline{\mathbf{A}}(\omega)] = 0 \quad (14)$$

In general, solving Eq. (14) for ω , gives complex frequencies. One way to calculate the natural frequencies is solving Eq. (14) numerically. Under certain approximations one can also obtain analytical formulas of resonance frequencies. Similarly, in [64] authors applied SDA to calculate the natural frequency of a dimer of particles made of metallic nanoshell and dielectric core for symmetric and anti-symmetric conditions. In the next section, we study only the rotationally symmetric magnetic resonance case by simplifying the Eq. (14) to a scalar equation and for the first time we provide a simple approximate formula to estimate the natural frequency and quality factor of clusters with an arbitrary number of metal nanospheres.

A. Magnetic Resonance Frequency

Owing to the rotational symmetry associated to a magnetic resonance in a cluster, each nanosphere induces a circulating displacement current resulting in the rotationally symmetric electric dipole moment disposition shown in Fig. 2. This resonance generates the overall longitudinal magnetic dipole moment of the cluster provided in Eq. (10). Therefore, owing to symmetry, we reduce the system in Eq. (12) made of $3N$ equations to a single scalar equation. This is because each sphere has identical induced electric dipole moment amplitude p_φ and polarized along the $\hat{\boldsymbol{\phi}}_n$ direction as $\mathbf{p}_n = p_\varphi \hat{\boldsymbol{\phi}}_n$.

Thus, the local electric field at the n^{th} nanosphere is written as $\mathbf{E}^{\text{loc}}(\mathbf{r}_n) = (p_\varphi/\alpha) \hat{\boldsymbol{\phi}}_n$. So, Eq. (11) is written as

$$(p_\varphi/\alpha) \hat{\boldsymbol{\phi}}_n - \sum_{\substack{m=1 \\ m \neq n}}^N \underline{\mathbf{G}}(\mathbf{r}_n, \mathbf{r}_m) \cdot p_\varphi \hat{\boldsymbol{\phi}}_m = \mathbf{E}^i(\mathbf{r}_n) \quad (15)$$

Natural frequencies are solution of Eq. (15) without excitation wave ($\mathbf{E}^i = 0$). By dividing all vector terms in Eq. (15) by $\alpha^{-1} p_\varphi$ and projecting the vectors in Eq. (15) on $\hat{\boldsymbol{\phi}}_n$ we obtain

$$1 - \sum_{\substack{m=1 \\ m \neq n}}^N \alpha \hat{\boldsymbol{\phi}}_n \cdot \underline{\mathbf{G}}(\mathbf{r}_n, \mathbf{r}_m) \cdot \hat{\boldsymbol{\phi}}_m = 0 \quad (16)$$

In Sec. 4 the complex natural frequency solution of Eq. (16) are also calculated numerically.

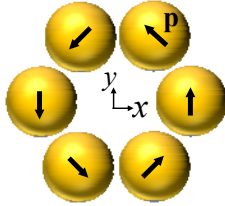


FIG. 2. The magnetic resonance has a symmetric disposition of electric dipoles along $\hat{\boldsymbol{\phi}}$, producing a strong magnetic field at the center.

A closed form formula for the complex natural frequency is obtained by applying some approximations. The first assumption is that both nanospheres and their mutual distances are sub-wavelength. Therefore, it is possible to replace the dynamic terms in both the polarizability and the Green's functions by the electrostatic ones. Which means the quasi static solution is equivalent to the limiting case where $k \rightarrow 0$ in Eq. (5) and Eq. (9), but keeping the correct frequency dependent dielectric constant ϵ_m in Eq. (6). The polarizability reduces to the Claussius-Mossotti relation [60]

$$\alpha \approx \alpha_0 = \frac{1}{2} \pi \epsilon_0 \epsilon_h d^3 \left(\frac{\epsilon_m - \epsilon_h}{\epsilon_m + 2\epsilon_h} \right) \quad (17)$$

The Green's function is approximated in the static regime as [61]

$$\underline{\mathbf{G}}(\mathbf{r}_n, \mathbf{r}_m) \approx \frac{1}{4\pi\epsilon_0\epsilon_h} \left[-\frac{1}{r_{nm}^3} \mathbf{I} + \frac{3}{r_{nm}^3} \hat{\mathbf{r}}_{nm} \hat{\mathbf{r}}_{nm} \right] \quad (18)$$

By substituting Eq. (17) and Eq. (18) in Eq. (16), after some algebraic manipulation Eq. (16) is reduced to

$$\epsilon_m = \frac{1+2L}{1-L} \epsilon_h \quad (19)$$

where $L = (2r_c/d)^3 / T$, and

$$T = \sum_{\substack{m=1 \\ m \neq n}}^N \left\{ \left(\frac{r_c}{r_{nm}} \right)^3 \left[\left(\frac{3A_{nm}}{D_{nm}} - 1 \right) \sin \varphi_n \sin \varphi_m + \right. \right. \\ \left. \left. - \frac{3B_{nm}}{D_{nm}} \sin(\varphi_n + \varphi_m) + \left(\frac{3C_{nm}}{D_{nm}} - 1 \right) \cos \varphi_n \cos \varphi_m \right] \right\} \quad (20)$$

In Eq. (20), A_{nm} , B_{nm} , C_{nm} and D_{nm} are the coefficients which relate the n^{th} nanosphere to the m^{th} one and are defined as

$$\begin{aligned} A_{nm} &= (\cos \varphi_n - \cos \varphi_m)^2 \\ B_{nm} &= (\cos \varphi_n - \cos \varphi_m)(\sin \varphi_n - \sin \varphi_m) \\ C_{nm} &= (\sin \varphi_n - \sin \varphi_m)^2 \\ D_{nm} &= A_{nm} + C_{nm} \end{aligned} \quad (21)$$

We are looking for complex natural angular frequency as $\omega = \omega' + i\omega''$. Substituting the Drude model for metal permittivity Eq. (6) into Eq. (19), and solving for ω , leads to the closed-form formula for complex natural angular frequency as

$$\omega' \approx \sqrt{\frac{\omega_p^2}{\epsilon_\infty - \frac{1+2L}{1-L} \epsilon_h} - \frac{\gamma^2}{4}}, \quad \omega'' \approx -\frac{\gamma}{2} \quad (22)$$

Note that Eq. (22) reduces to the natural frequency reported in [65] that was obtained for the specific case with $N = 4$ nanospheres.

It is important to note that with the quasi-static approximation, we neglect the radiation damping, therefore material loss (based on the Drude model) is the only remaining loss when evaluating these formulas. Since the natural frequency is complex, one can define the quality factor, as [66]

$$Q = -\frac{\omega'}{2\omega''} \quad (23)$$

A system with high quality factor provides a sharp resonance and strong overall magnetic dipole moment. According to the derived approximate formula for the natural frequency (Eq. (22)), we find an approximate formula for the quality factor of clusters with arbitrary number of nanospheres as

$$Q \approx \sqrt{\frac{(\omega_p/\gamma)^2}{\epsilon_\infty - \frac{1+2L}{1-L} \epsilon_h} - \frac{1}{4}} \quad (24)$$

where the number of nanospheres (N) is accounted for in the L parameter. In the next Section, we report the approximate (only material loss is considered) quality factor and natural frequency of the clusters of Fig. 1 with a comparison to the numerically found ones (both material loss and radiation loss are considered).

IV. RESULTS AND DISCUSSION

We address the effect of cluster parameters on the resonance frequency and on the two figures of merit F_H and F_γ introduced in Sec. 2. Studied structures include dimers, trimers, tetramers, pentamers, hexamers and octamers embedded in a host medium with relative permittivity $\epsilon_h = 2.25$ (it could represent the permittivity of an environment consisting of a glass substrate and a solution).

In the following, the magnetic resonance frequency is calculated using two distinct methods: (i) by solving Eq. (14) for complex frequency, in two ways: numerically, when the electric polarizability in Eq. (5) is used (denoted by $f_r(I)$ in Table 1) and by using the closed formula solution obtained via the approximate analytical method introduced in Sec. 3 (denoted as $f_r(II)$ in Table 1), and (ii) by finding the purely-real resonance frequency defined as the frequency that renders the magnetic field enhancement F_H maximum at the cluster center under time harmonic excitation (resonance denoted by $f_r(III)$ in Table 1). In this latter case, we assume the cluster illuminated by a single plane wave with electric field polarized along the y -axis and magnetic field along z , as shown in Fig. 3(a).

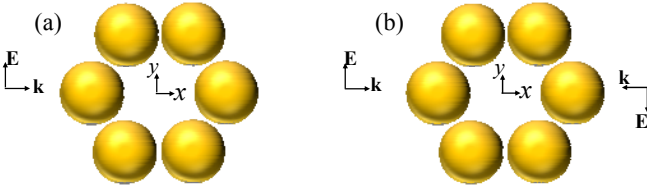


FIG. 3. Hexamer illuminated by (a) a single plane wave polarized along y axis, (b) a superposition of two counter-propagating plane waves with anti-symmetric electric field distribution with respect to the y - z plane, such that the electric field vanishes at the cluster center where a maximum of incident magnetic field is polarized along z .

In the reported comparisons of resonance frequencies calculated by different methods, we consider constant sphere diameter and gap in the clusters of Fig. 1 as 50 nm and 5 nm respectively. In fifth column of Table 1 we report F_H at the resonance frequency under single plane wave excitation. Finally, the quality factor Q based on the natural resonance frequency calculated numerically $f_r(I)$ and with the approximate formula $f_r(II)$ as in Eq. (22) are reported in the sixth and seventh columns of Table 1, respectively.

Furthermore, to provide a clear comparison among the methods, we define the percentage error in the real part of frequencies calculated numerically ($f_r'(I)$) and analytically (by approximate formula) ($f_r'(II)$) relative to $f_r(III)$ as

$$|e_r|\% = \left| \frac{f_r'(I \text{ or } II) - f_r(III)}{f_r(III)} \right| \times 100 \quad (25)$$

For the clusters reported in Table 1, the relative error for natural frequency calculated numerically ($f_r'(I)$) and approximately ($f_r'(II)$), is always less than 1% and 10% respectively. The very good agreement between $f_r'(I)$ and $f_r'(III)$, is consistent with the high quality factor $Q(I)$, which means that the resonant mode is clearly excited and well defined even by single plane wave excitation (we recall that to purely excite the magnetic resonance, two counter propagating plane waves need to be used, otherwise the single plane wave excites also other cluster modes). Note also that our approximate formula Eq. (22) provides a good estimate of resonance frequency. Moreover, by looking at the magnetic field enhancement F_H and the quality factor Q calculated numerically and approximately, two things can be inferred, (i) our approximate formula for quality factor works as a tool to show how strong the magnetic nanoantenna enhances the magnetic field, (ii) as the number of elements in a cluster increases, the magnetic field enhancement at the cluster center, and the quality factor decrease.

As shown in the Appendix A, for a cluster with a number of nanospheres N , assuming the resonance is made of N induced electric dipole moments perfectly polarized along $\hat{\phi}$ as shown in Fig. 2, the ratio of *scattered* power to the *absorbed* power is proportional to $P^{scat} / P^{abs} \propto N / \sin^2(\pi/N)$. This means that when N increases, for the magnetic resonance in these clusters, the loss due to scattering (as a magnetic dipole) is larger than the loss in the nanospheres. Hence, when the cluster is enlarged by adding more nanospheres (whereas the diameter of each nanosphere and the gap between them is fixed), the quality factor calculated numerically ($Q(I)$) (which is based on both material and radiation loss) drops more rapidly than the one calculated approximately ($Q(II)$) (which is only based on material loss).

Table 1. Comparison of natural frequencies found with different methods and the quality factor of different clusters of gold nanospheres when $d = 50$ nm and $g = 5$ nm

Cluster	$f_r(I)$ THz $f_r' + if_r''$	$f_r(II)$ THz $f_r' + if_r''$	$f_r(III)$ THz	F_H	$Q(I)$	$Q(II)$
$N=2$	566- i10 $ e_r = 0.1\%$	564-i8 $ e_r = 0.2\%$	566	9	28.6	33.8
$N=3$	538 - i10 $ e_r = 0.2\%$	540 - i8 $ e_r = 0.5\%$	537	6.7	26.6	32.3
$N=4$	513- i11 $ e_r = 0.4\%$	523-i8 $ e_r = 2\%$	511	7.1	22.6	31.3
$N=5$	494- i13 $ e_r = 0.3\%$	513-i8 $ e_r = 4\%$	492	6.5	18.9	30.7
$N=6$	479- i15 $ e_r = 0.3\%$	506-i8 $ e_r = 6\%$	477	5.8	15.6	30.3
$N=8$	456 -i21 $ e_r = 1\%$	500-i8 $ e_r = 10\%$	452	4.5	10.8	29.9

Next, in Fig. 4 we explore the effect of the nanospheres' diameter d and gap spacing g on the magnetic field enhancement F_H (evaluated at the cluster center at its resonance frequency) for the clusters shown in Fig. 1.

We excite each cluster with a single plane wave polarized along the y -direction as shown in Fig. 3(a). For each cluster the nanosphere diameter varies from 5 nm to 90 nm and the

gap varies from 1 nm to 20 nm. Note that the resonance frequency is not constant when varying d and g , therefore in Fig. 4 we superimpose some of the iso-frequency contours denoting the resonance frequency at which F_H is given.

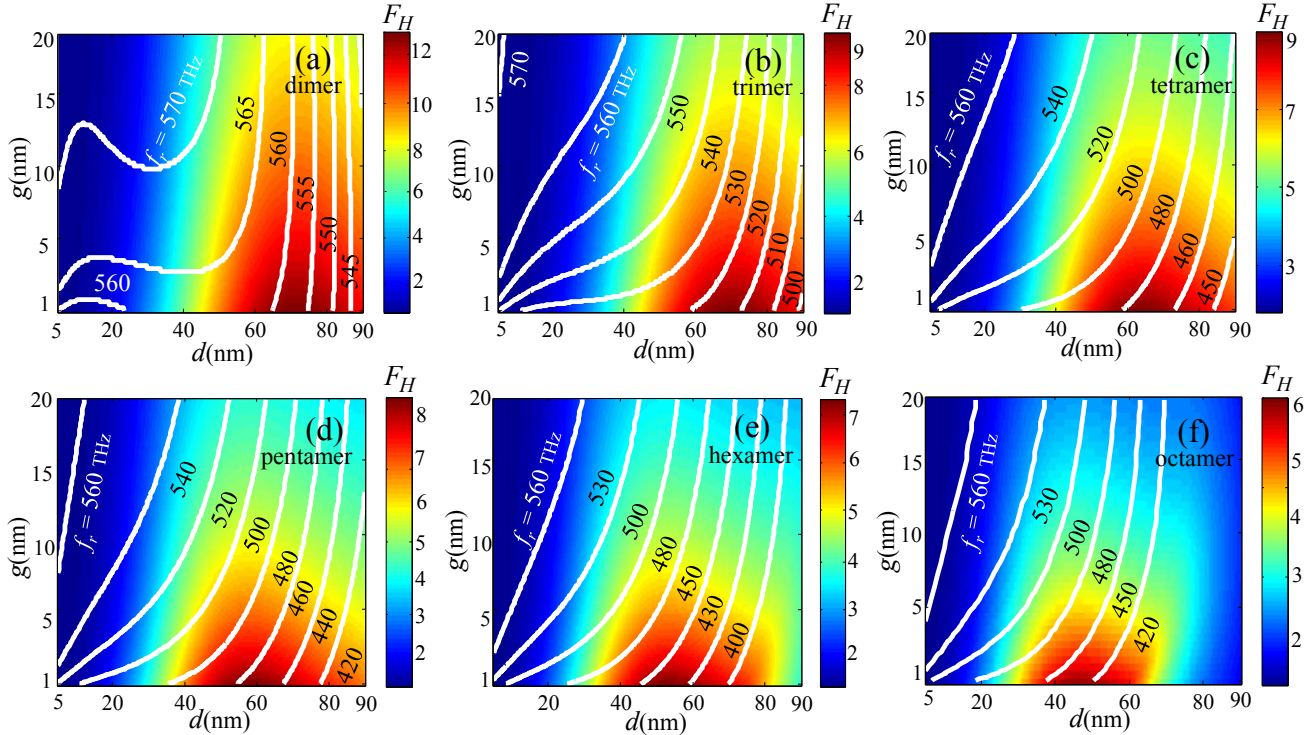


FIG. 4. Magnetic field enhancement F_H at the center of each cluster at its resonance frequency for: (a) dimer, (b) trimer, (c) tetramer (d) pentamer (e) hexamer (f) octamer. Nanospheres' diameter d and gap g vary between 5 and 90 nm and between 1 and 20 nm, respectively. Each cluster is excited by a single plane wave polarized along the y axis.

Results shown in Fig. 4 verify the important conclusion that as the cluster's number of nanospheres increases, the magnetic field enhancement at its center decreases. Furthermore, according to Fig. 4, for a given N and g , the magnetic field enhancement at the cluster center increases by increasing the nanosphere diameter, till it reaches a maximum for an optimum diameter, and if the diameter is further increased F_H decreases. Moreover, according to Fig. 4 for a given sphere diameter, F_H decreases by increasing the gap space between two adjacent nanospheres.

Fig. 5 shows the normalized local field admittance F_Y at the center of a hexamer evaluated at its resonance frequency, which depends on the varying parameters d and g . According to Fig. 5 the effect of diameter and gap on the local field admittance at the center of hexamer, is the same as the magnetic field enhancement case, i.e. for a certain nanosphere diameter increasing the gap, causes decrease in F_Y and for a specific gap, increasing the diameter causes increase in F_Y till it reaches the optimum diameter after which by increasing the diameter, F_Y decreases. Another important conclusion from Fig. 5 is that with single plane wave excitation, the local field admittance at the cluster center is not large, which means with this type of excitation, the cluster is not able to create a strong magnetic dominant region. This is a motivation to change the excitation beam to superposition of two counter-propagating plane waves to eliminate the electric field at the cluster center and enhance the local field admittance, as shown in Fig. 10.

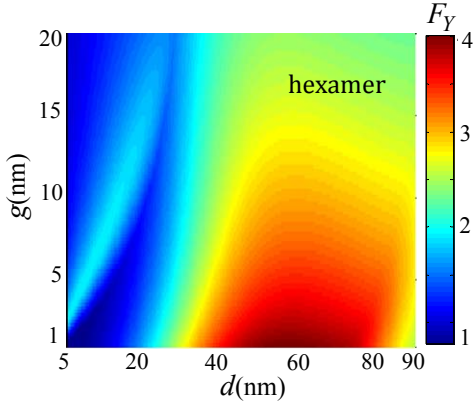


FIG. 5. Local field admittance (F_Y) at the center of a hexamer when d and g vary in the ranges 5-90 nm and 1-20 nm, respectively. The hexamer is excited by a single plane wave polarized along the y axis.

Since circular clusters produce circulating currents, the radius of the cluster plays an important role in characterizing the magnetic response. As it is clear from Fig. 4, for each cluster there are many pairs of d and g (but different cluster radius r_c) that yield the same resonance frequency and different magnetic field enhancement. To investigate the effect of cluster radius on the magnetic field enhancement (Fig. 6), we use Fig. 4 to extract information about resonating

clusters at a certain resonance frequency (here we choose 480 THz, since most of the clusters have resonance at this frequency). Fig. 6 represents the magnetic field enhancement (F_H) at the cluster center versus radius of cluster (r_c) for clusters with various number of nanospheres which resonate at 480 THz. It is worth mentioning that for each cluster with specific number of nanospheres (N) resonating at 480 THz, there is an optimum cluster radius at which the magnetic field enhancement is maximized. Moreover, when the number of nanospheres in a cluster increases, the optimum radius of the cluster increases and its corresponding magnetic field enhancement reduces.

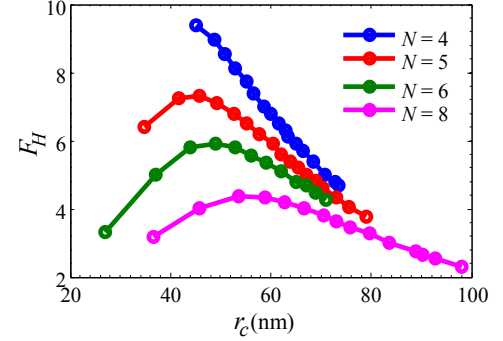


FIG. 6. Magnetic field enhancement (F_H) at the center of a cluster versus cluster's radius for different cases on particle numbers N . In all cases geometries are chosen so clusters resonate at 480 THz.

As mentioned earlier, to create a magnetic dominant region, one needs to establish symmetry conditions on both the cluster and the incident field such that the net electric response of the cluster is suppressed. The clusters we introduced so far are rotationally symmetric and host strong magnetic dipolar mode. Moreover, by applying two counter-propagating plane waves with anti-symmetric electric field distribution with respect to cluster symmetry plane (y - z plane in our structure) as shown in Fig. 3(b), the external electric field vanishes and due to the clusters rotational symmetry, no net electric field is created at the cluster center. This excitation method leads to strong electric field in the gap region between nanospheres and strong magnetic field at the cluster center. Our findings (for brevity details not shown here) show that for the clusters studied in this paper, the magnetic field enhancement defined as in Eq. (1) does not depend on the excitation type, i.e., a single plane wave versus two counter-propagating plane waves as in Fig. 3(b). With two counter-propagating plane waves illumination, for each cluster, we study the behavior of magnetic field enhancement, with respect to frequency, based on both the analytical formulation using SDA and full wave simulations. Full wave simulations are performed by the frequency domain finite elements method (FEM), implemented in the commercial software CST Microwave Studio by Computer Simulation Technology AG. Fig. 7 shows the magnetic field enhancement (F_H) versus frequency for clusters shown in Fig. 1, at the cluster center, by using SDA [Fig. 7(a)] and full wave simulations [Fig. 7(b)] when the diameter of each nanosphere and the gap spacing are kept

constant as 50 nm and 5 nm, respectively and the clusters are excited by two counter-propagating plane waves as shown in Fig.3 (b).

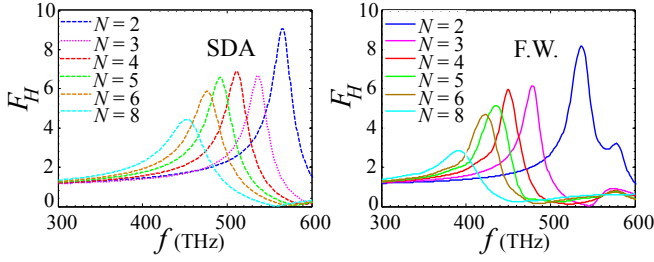


FIG. 7. Magnetic field enhancement at the cluster center versus frequency for different cluster sizes. Results are calculated via (a) SDA analysis and via (b) full wave (F.W.) simulations. In each case the cluster is excited by two counter-propagating plane waves as in Fig. 3(b).

Fig. 7 confirms that both analysis methods lead to the same conclusion that enlarging the cluster by adding more nanospheres results in reducing the magnetic field enhancement *at the cluster center*, red shifting the resonance frequency and increasing the resonance line width. There is a slight difference between the resonance frequencies obtained with full wave simulation and those obtained with SDA (5% in the dimer case and increasing to 15% in the octamer case). SDA calculations also overestimate the magnetic field enhancement by 8% in the trimer case and up to by 50% in the octamer case. The difference between the results obtained with these two methods, grows as the number of nanospheres increases. This difference originates from the fact that in SDA we neglect the magnetic dipole moment of each nanosphere and also all higher order multipoles, and by adding more nanospheres in a cluster, the effect is cumulative. To elaborate on this issue, we study also the absorption [Fig. 8(a-b)], scattering [Fig. 8 (c-d)], and extinction [Fig. 8(e-f)] cross sections of the clusters shown in Fig. 1 based on equations given in Appendix B. These cross sections are evaluated using both the SDA [Fig. 8(a, c, e)] and full wave simulations [Fig. 8(b, d, f)] assuming the diameter of each nanosphere and the gap spacing to be constant as 50 nm and 5 nm, respectively. In these simulations clusters are excited by two counter-propagating plane waves as shown in Fig. 3(b). In each plot, the cross sections are normalized to the geometrical cross section of a single nanosphere $\sigma_g = \pi(d/2)^2$. At the magnetic resonance, each cluster exhibits a peak in the absorption and scattering, and hence in the extinction cross section. Moreover, according to the cross sections specifically obtained by full wave simulations, we observe that adding more nanospheres in a cluster leads to larger cross section. Furthermore, since the scattering cross section is proportional to the total magnetic dipole moment of the cluster, as the number of nanospheres increases, stronger magnetic dipole moment is achieved. We used two counter-propagating plane waves excitation since it facilitates the simulation burden and it makes the electric dipole moment vanish. Higher order multipoles like the electric quadrupole are still present, though weak compared to the magnetic dipole since each of these

simulations are carried out at the magnetic resonance frequency. Effects of the electric quadrupole are visible at higher frequencies in the simulations, analogously to what was shown in detail in Figs. 3-5 of [32] for spherical clusters. Note that higher order multipoles are not visible in the scattering cross section calculated with the SDA since it is evaluated in an approximate way (Eq. (A5) by considering only the scattering due to a magnetic dipole).

Results also confirm the trend already observed in Fig. 7: as we increase the number of the nanospheres in the cluster the results of the SDA diverge from those of full-wave simulations.

simulations are carried out at the magnetic resonance frequency. Effects of the electric quadrupole are visible at higher frequencies in the simulations, analogously to what was shown in detail in Figs. 3-5 of [32] for spherical clusters. Note that higher order multipoles are not visible in the scattering cross section calculated with the SDA since it is evaluated in an approximate way (Eq. (A5) by considering only the scattering due to a magnetic dipole).

Results also confirm the trend already observed in Fig. 7: as we increase the number of the nanospheres in the cluster the results of the SDA diverge from those of full-wave simulations.

Results also confirm the trend already observed in Fig. 7: as we increase the number of the nanospheres in the cluster the results of the SDA diverge from those of full-wave simulations.

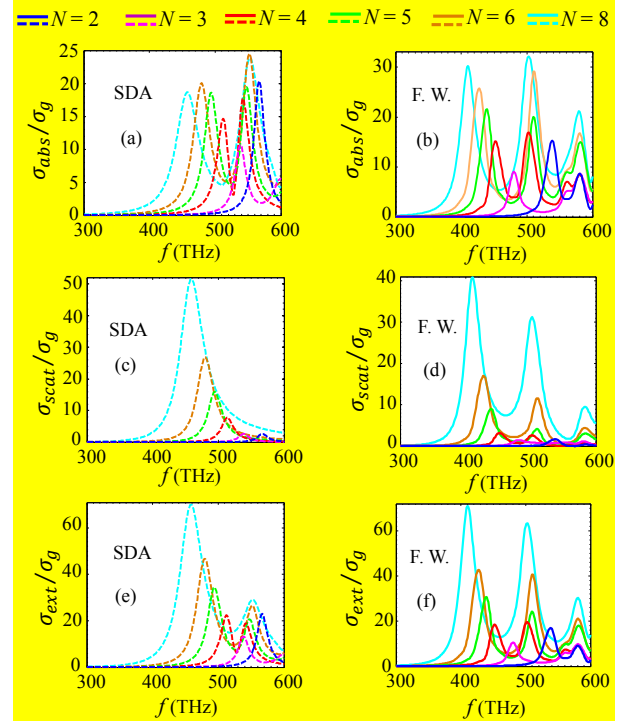


FIG. 8. Normalized absorption (a-b), scattering (c-d) and extinction (e-f) cross sections of clusters versus frequency, for different cluster sizes. Cross sections are normalized with respect to the geometrical cross section of a single nanosphere $\sigma_g = \pi(d/2)^2$. Results are calculated via SDA analysis (a, c, e) and via full wave (F.W.) simulations (b, d, f). In all cluster cases, the nanospheres' diameter and gaps are kept constant as 50 nm and 5 nm respectively. In each case the cluster is excited by two counter-propagating plane waves as in Fig. 3(b).

Although the magnetic field enhancement reduces at the cluster center as the cluster expands, to elaborate on the possible advantages of large clusters, we provide the magnetic field enhancement profile in the x - y plane for different clusters at their resonance frequency. Fig. 9(a-f) represents the magnetic field enhancement (F_H) profile in logarithmic scale (as $10 \log_{10}(F_H)$) the color legend is saturated for the values more than 10.4) calculated using SDA analysis for clusters represented in Fig. 1 when the nanospheres' diameter and gap between them are kept constant as 50 nm and 5 nm respectively and the clusters are excited by two counter-propagating plane waves as shown in Fig. 3(b), at their

resonance frequency obtained from Fig. 7(a). According to Fig. 9, the magnetic field enhancement at the gap space between adjacent nanospheres is always strong and it is slightly stronger near the nanospheres rather than at the cluster center. Moreover, as the number of nanospheres in the cluster increases, the area with strong magnetic field becomes wider. According to Table 1 the quality factor decreases with size which results in the reduction of the magnetic field enhancement at the cluster center. Therefore, there is always a trade-off between getting the maximum magnetic field enhancement at a certain point such as the center of a cluster

and having strong magnetic field over a wide area inside the cluster. Plots in Fig. 9 show also a strong magnetic field enhancement outside the cluster with the shape of two vertical bands (dark red bands with extraordinary large F_H). This is due to the specific excitation used in Fig. 9 with two counter-propagating plane waves shown in Fig. 3(b) that form a standing wave pattern of the incident magnetic field. There are two nulls with half a wavelength distance and result in locally huge magnetic field enhancement [49].

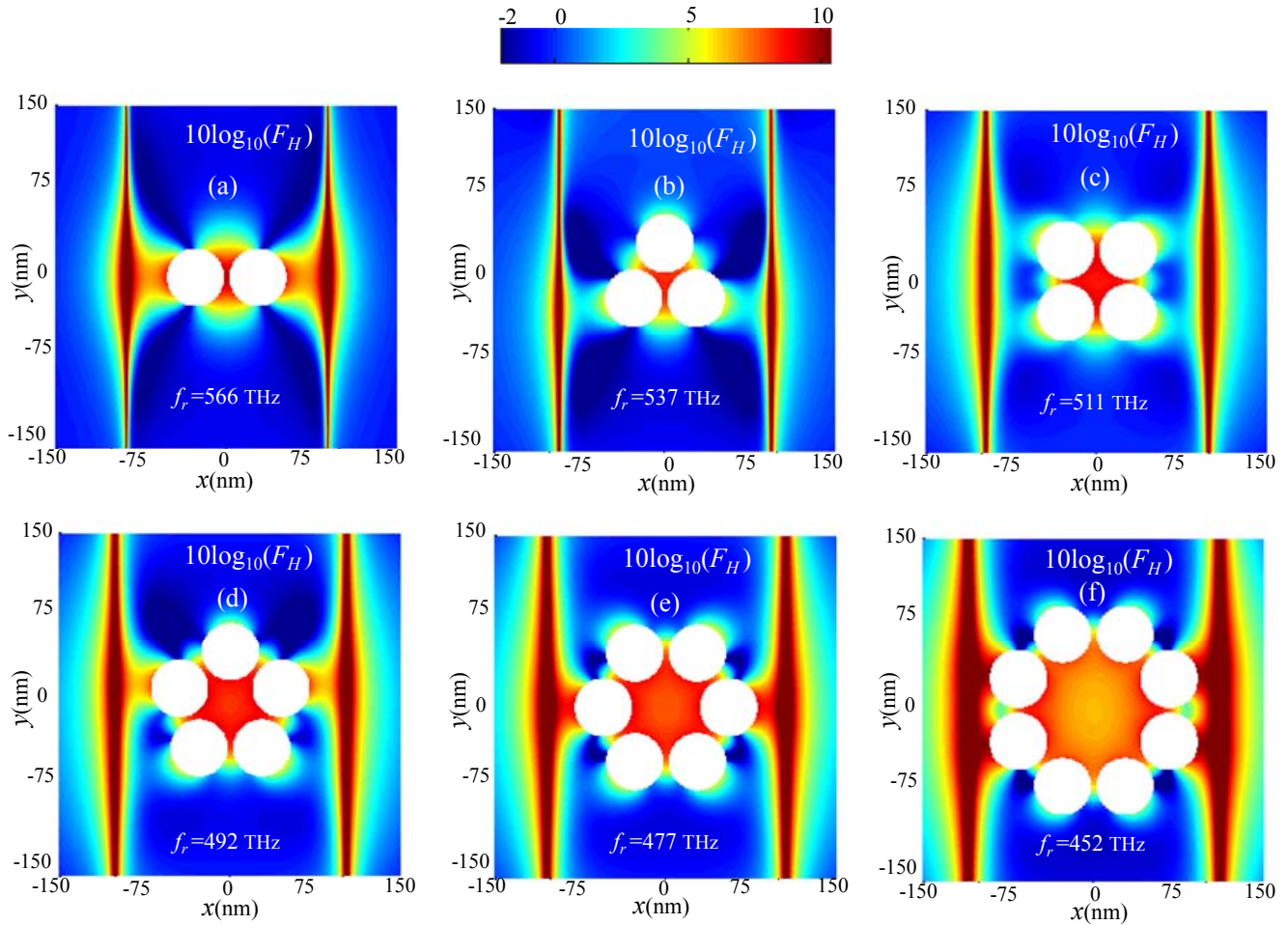


FIG. 9. Magnetic field enhancement (F_H) profile in logarithmic scale (as $10\log_{10}(F_H)$), the color legend is saturated for the values more than 10.4) of (a) dimer, (b) trimer, (c) tetramer, (d) pentamer, (e) hexamer, (f) octamer with $d = 50$ nm and $g = 5$ nm. Each cluster is excited with two counter-propagating plane waves with anti-symmetric electric field with respect to the $y-z$ plane.

Furthermore, to demonstrate the advantage of the symmetric excitation method (as shown in Fig. 3(b)) and to create the magnetic dominant region with low electric field, we investigate the local field admittance (F_Y) profile in the $x-y$ plane when the clusters are excited with two counter-propagating plane waves as in Fig. 3(b). Fig. 10(a-f) shows the

local field admittance profile in logarithmic scale (the color legend is saturated for the values more than 4) calculated using SDA method for clusters shown in Fig. 1 with fixed diameter and gap of 50 nm and 5 nm respectively, while the clusters are excited with two counter-propagating plane waves with anti-symmetric electric field with respect to the $y-z$ plane.

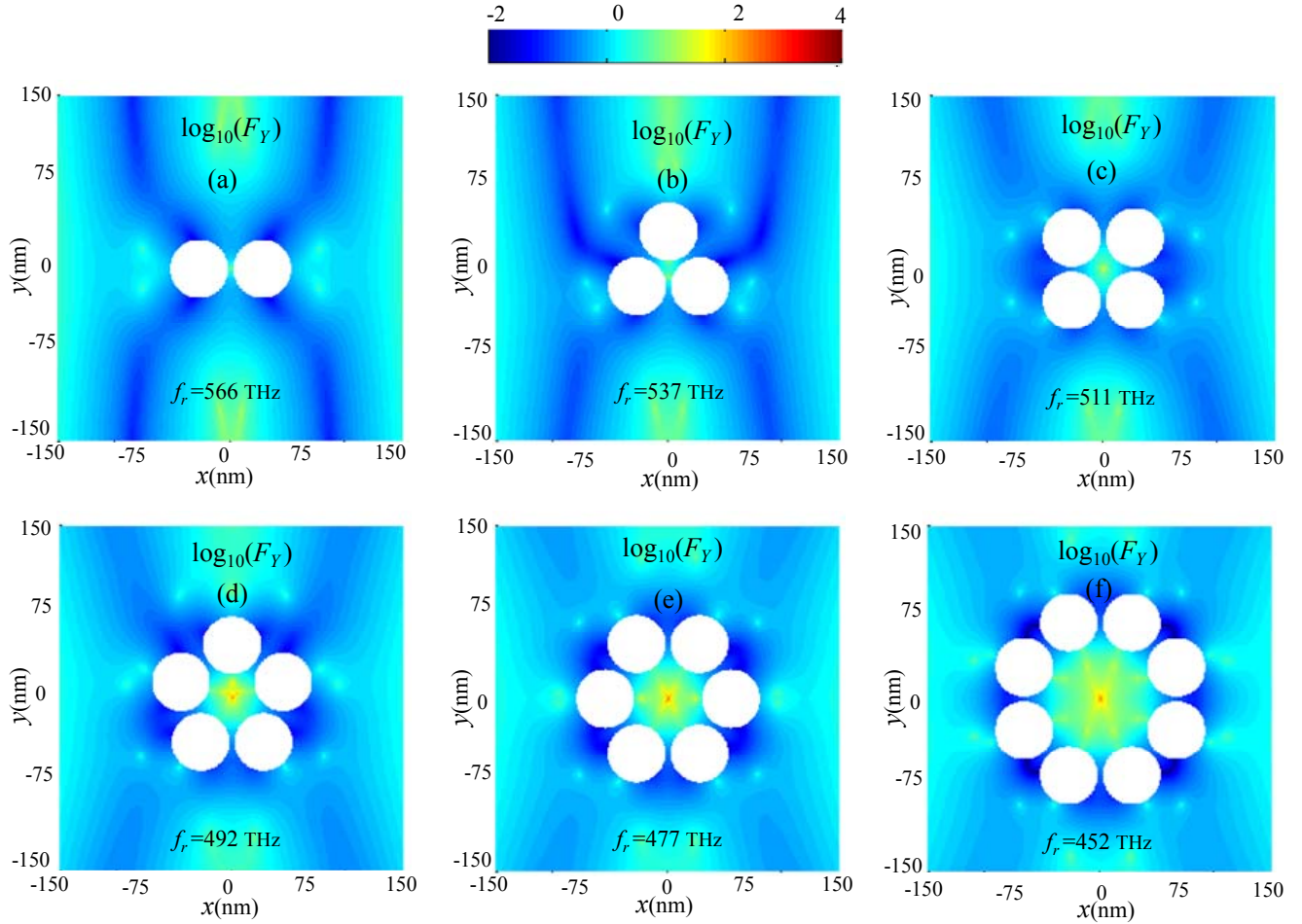


FIG. 10. The local field admittance (F_Y) profile of different clusters with $d = 50$ nm and $g = 5$ nm, in logarithmic scale (the color legend is saturated for the values more than 4, i.e., for $F_Y > 10^4$) (a) dimer, (b) trimer, (c) tetramer, (d) pentamer, (e) hexamer, (f) octamer. Each cluster is excited with two counter-propagating plane waves with anti-symmetric electric field with respect to the y - z plane. Results show a large magnetic field around the electric field ratio center.

Owing to the two counter-propagating plane waves excitation shown in Fig. 3(b), the incident electric fields cancel out exactly at the center of the cluster, so a giant local field admittance is expected at the center of each cluster. Moreover, enlarging the clusters by adding more nanospheres, leads to a wide area inside the cluster which possesses strong magnetic field (Fig. 9) and large field admittance (Fig. 10). In other words, there is a region of magnetic dominance. Furthermore, comparison of Fig. 10(e) and Fig. 5 for the case of $d = 50$ nm and $g = 5$ nm, clearly shows that the level of local field admittance is much higher when the clusters are excited by a symmetric excitation.

V. CONCLUSION

We have investigated clusters of gold nanospheres embedded in a host medium as magnetic nanoantennas to enhance the magnetic field at optical frequencies and we have shown how the electric field can be reduced at the cluster center. We sorted clusters based on their quality factor, the

magnetic field enhancement and their ability to create a wide magnetic dominant region. We applied SDA to calculate the total magnetic and electric field at an arbitrary point while the clusters were illuminated by two different methods of excitation: (i) single plane wave and (ii) superposition of two counter-propagating plane waves to eliminate the electric field at the cluster center where the magnetic field is enhanced. We provided for the first time, a formula to approximate the natural frequency of clusters and their quality factor with arbitrary number of elements. We also, calculated the natural frequency and quality factor numerically and demonstrated the validity range of our proposed formulation. We defined two figures of merit to study the magnetic nanoantennas efficacy: (i) magnetic field enhancement (F_H) which shows the ability of the nanoantenna to enhance the magnetic field and (ii) the local field admittance (F_Y) which shows how much the magnetic field is enhanced compared to the electric field. We verified our analytic results against full wave simulations and showed their consistency. The results indicated three facts about the clusters of nanospheres as

magnetic nanoantennas: (i) increasing the number of elements in a cluster, leads to red shift in resonance frequency, decrease in quality factor and the level of magnetic field enhancement at the center of cluster whereas the area of magnetic dominant region increases; (ii) in each cluster, increasing the diameter of spheres first causes stronger enhancement and there is an optimum diameter after which the enhancement reduces by further increasing the diameter. (iii) increasing the gap spacing in a cluster, causes less magnetic field enhancement at the cluster center. According to our study, clusters of gold nanospheres, because of their symmetry, when illuminated by a symmetric excitation are good magnetic nanoantennas with large magnetic to electric field ratio at the center.

ACKNOWLEDGMENT

Authors acknowledge support from the W. M. Keck Foundation, USA, and from the National Science Foundation, NSF-SNM-1449397. The authors are grateful to CST Simulation Technology AG for letting them use the simulation tool CST Microwave Studio that was instrumental in this analysis.

APPENDIX A: RADIATED AND ABSORBED POWER BY A CLUSTER

We assume that for a resonating cluster with N nanospheres, the magnetic resonance has a symmetric disposition of electric dipoles as shown in Fig. 2. Hence all the N electric dipoles are polarized along the $\hat{\phi}$ direction and have equal magnitude p_ϕ . According to [67,68], the absorbed time-average power in the n^{th} nanosphere of the cluster is

$$P_n^{abs} = \frac{\omega \epsilon_0 \epsilon_h}{2} \left[\frac{\text{Im}(\alpha)}{\epsilon_0 \epsilon_h} - \frac{k^3}{6\pi(\epsilon_0 \epsilon_h)^2} |\alpha|^2 \right] |\mathbf{E}^{loc}(\mathbf{r}_n)|^2 \quad (26)$$

where α is the polarizability of each nanosphere given in Eq. (5). Moreover, since we assume that at resonance $\mathbf{E}^{loc}(\mathbf{r}_n) = (p_\phi/\alpha) \hat{\phi}_n$, Eq. (A1) reads

$$P_n^{abs} = -\frac{\omega}{2} \left[\text{Im}\left(\frac{1}{\alpha}\right) + \frac{k^3}{6\pi\epsilon_0\epsilon_h} \right] |p_\phi|^2 \quad (27)$$

Owing to the circular symmetry of the dipoles' strength, the total cluster power lost due to absorption is

$$P^{abs} = \sum_{n=1}^N P_n^{abs} = -\frac{\omega N}{2} \left[\text{Im}\left(\frac{1}{\alpha}\right) + \frac{k^3}{6\pi\epsilon_0\epsilon_h} \right] |p_\phi|^2 \quad (28)$$

According to Eq. (10), and because of the symmetry of the magnetic resonance, the overall magnetic dipole moment of the cluster with N nanospheres when the cluster center is at the origin is

$$\mathbf{m} = -\frac{i\omega}{2} r_c p_\phi N \hat{\mathbf{z}} \quad (29)$$

where r_c is the radius of the cluster, defined in Eq. (3). The scattered power by the cluster is evaluated as the power scattered by a magnetic dipole moment leading to [69]

$$P^{scat} = \frac{\omega}{2} \frac{k^3 \mu_0^2}{6\pi\epsilon_0\epsilon_h} \frac{|\mathbf{m}|^2}{\eta^2} \quad (30)$$

where we have neglected the power contributions associated to higher order multipoles. By substituting Eq. (A4) into Eq. (A5), the total scattered power by the cluster is

$$P^{scat} = \frac{\omega^5}{48\pi} k \epsilon_0 \epsilon_h \mu_0^2 r_c^2 N^2 |p_\phi|^2 \quad (31)$$

If we assume that in a cluster with N nanospheres, the diameter of each nanosphere and the gap between them is kept constant when varying N , by substituting the expression for the cluster radius in Eq. (3) into Eq. (A6), the ratio of scattered power by a cluster to the absorbed power is

$$\frac{P^{scat}}{P^{abs}} = \frac{N}{\sin^2(\pi/N)} \frac{\omega^4}{96\pi} \frac{k \epsilon_0 \epsilon_h \mu_0^2 (d+g)^2}{\left[\text{Im}\left(\frac{1}{\alpha}\right) + \frac{k^3}{6\pi\epsilon_0\epsilon_h} \right]} \quad (32)$$

Moreover, one can substitute the Drude model permittivity provided in Eq. (6), into the electric polarizability (Eq. (5)), then the ratio of the scattered power by a cluster to the absorbed power is written as

$$\frac{P^{scat}}{P^{abs}} = \frac{N}{\sin^2(\pi/N)} Z \quad (33)$$

where

$$Z = \frac{\omega^3 \epsilon_0^2 \epsilon_h \mu_0^2 k \pi d^3 (d+g)^2}{576} \left\{ \frac{[\omega^2(\epsilon_\infty - \epsilon_h) - \epsilon_\infty \omega_p^2]^2}{\gamma \epsilon_\infty \omega_p^2} + \frac{\gamma^2 \omega^2 (\epsilon_\infty - \epsilon_h)^2}{\gamma \epsilon_\infty \omega_p^2} \right\} \quad (34)$$

APPENDIX B: ABSORPTION, SCATTERING AND EXTINCTION CROSS SECTIONS

According to [70], the absorption, scattering and extinction cross sections are defined as

$$\sigma_{abs} = \frac{\sum_{n=1}^N P_n^{abs}}{S^i}, \quad \sigma_{scat} = \frac{P^{scat}}{S^i} \quad (B1)$$

and $\sigma_{ext} = \sigma_{abs} + \sigma_{scat}$. Here P_n^{abs} and P^{scat} are calculated using Eq. (A1) and Eq. (A5), and $S^i = \frac{\eta}{2} |\mathbf{H}^i|^2$, where $|\mathbf{H}^i|$ is the magnitude of the *total* incident magnetic field exciting the cluster meta-particle. Note that we are focusing on the

magnetic dipole excitation of a cluster that is seen here as a single scattering and absorbing meta-particle. Indeed, scattering of a particle described by its magnetic dipole is proportional to $|\mathbf{m}|^2 = |\alpha_m^{eff} \mathbf{H}^i|^2$ (α_m^{eff} is the effective magnetic polarizability of the cluster meta-particle) as shown in Eq. (A5), and its absorption is proportional to $\text{Im}\{\mathbf{m} \cdot \mathbf{H}^{i*}\} \propto |\mathbf{H}^i|^2$, where the asterisk * denotes complex conjugation. This case is analogous to that of a particle described by its electric dipole absorption and scattering that

$$S^i = \frac{1}{2\eta} |\mathbf{E}^i|^2$$

would be proportional to $\frac{1}{2\eta} |\mathbf{E}^i|^2$. Note that in our simulations where we use an excitation made of two counter-propagating plane waves (as shown in Fig. 3(b)), S^i defined above is equivalent to $S^i = 4\hat{\mathbf{k}}^{pw} \cdot \frac{1}{2} \text{Re}\{\mathbf{E}^{pw} \times \mathbf{H}^{pw*}\} = 4\frac{\eta}{2} |\mathbf{H}^{pw}|^2$, where $\hat{\mathbf{k}}^{pw}$ is normalized wavevector of either plane wave and \mathbf{E}^{pw} and \mathbf{H}^{pw} are its electric and magnetic fields. For the case of two counter-propagating plane waves considered in Fig. 3(b) we have $\mathbf{H}^i = 2\mathbf{H}^{pw}$ and $\mathbf{E}^i = 0$ at the cluster center where we assume the equivalent magnetic dipole is located.

-
- [1] M. Burrese, D. van Oosten, T. Kampfrath, H. Schoenmaker, R. Heideman, A. Leinse, and L. Kuipers, Probing the Magnetic Field of Light at Optical Frequencies, *Science* **326**, 550 (2009).
- [2] H. Giessen and R. Vogelgesang, Glimpsing the Weak Magnetic Field of Light, *Science* **326**, 529 (2009).
- [3] T. H. Taminiau, S. Karaveli, N. F. van Hulst, and R. Zia, Quantifying the Magnetic Nature of Light Emission, *Nat. Commun.* **3**, 979 (2012).
- [4] M. Kasperczyk, S. Person, D. Ananias, L. D. Carlos, and L. Novotny, Excitation of Magnetic Dipole Transitions at Optical Frequencies, *Phys. Rev. Lett.* **114**, 163903 (2015).
- [5] A. Alu and N. Engheta, The Quest for Magnetic Plasmons at Optical Frequencies, *Opt. Express* **17**, 5723 (2009).
- [6] P. Albella, M. A. Poyli, M. K. Schmidt, S. A. Maier, F. Moreno, J. J. Sáenz, and J. Aizpurua, Low-Loss Electric and Magnetic Field-Enhanced Spectroscopy with Subwavelength Silicon Dimers, *J. Phys. Chem. C* **117**, 13573 (2013).
- [7] L. Zou, W. Withayachumnankul, C. M. Shah, A. Mitchell, M. Bhaskaran, S. Sriram, and C. Fumeaux, Dielectric Resonator Nanoantennas at Visible Frequencies, *Opt. Express* **21**, 1344 (2013).
- [8] G. N. Malheiros-Silveira, G. S. Wiederhecker, and H. E. Hernández-Figueroa, Dielectric Resonator Antenna for Applications in Nanophotonics, *Opt. Express* **21**, 1234 (2013).
- [9] R. Verre, Z. J. Yang, T. Shegai, and M. Käll, Optical Magnetism and Plasmonic Fano Resonances in Metal–Insulator–Metal Oligomers, *Nano Lett.* **15**, 1952 (2015).
- [10] R. S. Savelev, S. V. Makarov, A. E. Krasnok, and P. A. Belov, From Optical Magnetic Resonance to Dielectric Nanophotonics (A Review), *Opt. Spectrosc.* **119**, 551 (2015).
- [11] D. Markovich, K. Baryshnikova, A. Shalin, A. Samusev, A. Krasnok, P. Belov, and P. Ginzburg, Enhancement of Artificial Magnetism via Resonant Bianisotropy, *Sci. Rep.* **6**, (2016).
- [12] T. J. Yen, W. J. Padilla, N. Fang, D. C. Vier, D. R. Smith, J. B. Pendry, D. N. Basov, and X. Zhang, Terahertz Magnetic Response from Artificial Materials, *Science* **303**, 1494 (2004).
- [13] J. D. Baena, R. Marqués, F. Medina, and J. Martel, Artificial Magnetic Metamaterial Design by Using Spiral Resonators, *Phys. Rev. B* **69**, 014402 (2004).
- [14] A. N. Lagarkov and A. K. Sarychev, Electromagnetic Properties of Composites Containing Elongated Conducting Inclusions, *Phys. Rev. B* **53**, 6318 (1996).
- [15] G. Dolling, C. Enkrich, M. Wegener, J. F. Zhou, C. M. Soukoulis, and S. Linden, Cut-Wire Pairs and Plate Pairs as Magnetic Atoms for Optical Metamaterials, *Opt. Lett.* **30**, 3198 (2005).
- [16] S. Linden, C. Enkrich, G. Dolling, M. W. Klein, J. Zhou, T. Koschny, C. M. Soukoulis, S. Burger, F. Schmidt, and M. Wegener, Photonic Metamaterials: Magnetism at Optical Frequencies, *IEEE J. Sel. Top. Quantum Electron.* **12**, 1097 (2006).
- [17] C. M. Soukoulis, S. Linden, and M. Wegener, Negative Refractive Index at Optical Wavelengths, *Science* **315**, 47 (2007).
- [18] V. M. Shalaev, Optical Negative-Index Metamaterials, *Nat. Photonics* **1**, 41 (2007).
- [19] J. B. Pendry, A. J. Holden, D. J. Robbins, and W. J. Stewart, Magnetism from Conductors and Enhanced Nonlinear Phenomena, *IEEE Trans. Microw. Theory Tech.* **47**, 2075 (1999).
- [20] R. A. Shelby, D. R. Smith, and S. Schultz, Experimental Verification of a Negative Index of Refraction, *Science* **292**, 77 (2001).
- [21] K. Aydin, I. Bulu, K. Guven, M. Kafesaki, C. M. Soukoulis, and E. Ozbay, Investigation of Magnetic Resonances for Different Split-Ring Resonator Parameters and Designs, *New J. Phys.* **7**, 168 (2005).
- [22] J. Zhou, T. Koschny, M. Kafesaki, E. N. Economou, J. B. Pendry, and C. M. Soukoulis, Saturation of the Magnetic Response of Split-Ring Resonators at Optical Frequencies, *Phys. Rev. Lett.* **95**, 223902 (2005).
- [23] S. Linden, C. Enkrich, M. Wegener, J. Zhou, T. Koschny, and C. M. Soukoulis, Magnetic Response of Metamaterials at 100 Terahertz, *Science* **306**, 1351 (2004).
- [24] C. Enkrich, M. Wegener, S. Linden, S. Burger, L. Zschiedrich, F. Schmidt, J. F. Zhou, T. Koschny, and C. M. Soukoulis, Magnetic Metamaterials at

- Telecommunication and Visible Frequencies, *Phys. Rev. Lett.* **95**, 203901 (2005).
- [25] N. Katsarakis, G. Konstantinidis, A. Kostopoulos, R. S. Penciu, T. F. Gundogdu, M. Kafesaki, E. N. Economou, T. Koschny, and C. M. Soukoulis, Magnetic Response of Split-Ring Resonators in the Far-Infrared Frequency Regime, *Opt. Lett.* **30**, 1348 (2005).
- [26] T. D. Corrigan, P. W. Kolb, A. B. Sushkov, H. D. Drew, D. C. Schmadel, and R. J. Phaneuf, Optical Plasmonic Resonances in Split-Ring Resonator Structures: An Improved LC Model, *Opt. Express* **16**, 19850 (2008).
- [27] M. S. Wheeler, J. S. Aitchison, and M. Mojahedi, Three-Dimensional Array of Dielectric Spheres with an Isotropic Negative Permeability at Infrared Frequencies, *Phys. Rev. B* **72**, 193103 (2005).
- [28] S. Campione, S. Lannebère, A. Aradian, M. Albani, and F. Capolino, Complex Modes and Artificial Magnetism in Three-Dimensional Periodic Arrays of Titanium Dioxide Microspheres at Millimeter Waves, *JOSA B* **29**, 1697 (2012).
- [29] S. Campione, M. B. Sinclair, and F. Capolino, Effective Medium Representation and Complex Modes in 3D Periodic Metamaterials Made of Cubic Resonators with Large Permittivity at Mid-Infrared Frequencies, *Photonics Nanostructures - Fundam. Appl.* **11**, 423 (2013).
- [30] S. Lannebère, S. Campione, A. Aradian, M. Albani, and F. Capolino, Artificial Magnetism at Terahertz Frequencies from Three-Dimensional Lattices of TiO₂ Microspheres Accounting for Spatial Dispersion and Magnetolectric Coupling, *JOSA B* **31**, 1078 (2014).
- [31] C. R. Simovski and S. A. Tretyakov, Model of Isotropic Resonant Magnetism in the Visible Range Based on Core-Shell Clusters, *Phys. Rev. B* **79**, 045111 (2009).
- [32] A. Vallecchi, M. Albani, and F. Capolino, Collective Electric and Magnetic Plasmonic Resonances in Spherical Nanoclusters, *Opt. Express* **19**, 2754 (2011).
- [33] S. Mühlig, A. Cunningham, S. Scheeler, C. Pacholski, T. Bürgi, C. Rockstuhl, and F. Lederer, Self-Assembled Plasmonic Core-Shell Clusters with an Isotropic Magnetic Dipole Response in the Visible Range, *ACS Nano* **5**, 6586 (2011).
- [34] A. Vallecchi, M. Albani, and F. Capolino, Effect of Irregularities of Nanosatellites Position and Size on Collective Electric and Magnetic Plasmonic Resonances in Spherical Nanoclusters, *Opt. Express* **21**, 7667 (2013).
- [35] Z. Qian, S. P. Hastings, C. Li, B. Edward, C. K. McGinn, N. Engheta, Z. Fakhraei, and S.-J. Park, Raspberry-like Metamolecules Exhibiting Strong Magnetic Resonances, *ACS Nano* **9**, 1263 (2015).
- [36] S. Campione and F. Capolino, Electromagnetic Coupling and Array Packing Induce Exchange of Dominance on Complex Modes in 3D Periodic Arrays of Spheres with Large Permittivity, *JOSA B* **33**, 261 (2016).
- [37] D. K. Morits and C. R. Simovski, Negative Effective Permeability at Optical Frequencies Produced by Rings of Plasmonic Dimers, *Phys. Rev. B* **81**, 205112 (2010).
- [38] A. Alù, A. Salandrino, and N. Engheta, Negative Effective Permeability and Left-Handed Materials at Optical Frequencies, *Opt. Express* **14**, 1557 (2006).
- [39] M. Hentschel, M. Saliba, R. Vogelgesang, H. Giessen, A. P. Alivisatos, and N. Liu, Transition from Isolated to Collective Modes in Plasmonic Oligomers, *Nano Lett.* **10**, 2721 (2010).
- [40] B. Luk'yanchuk, N. I. Zheludev, S. A. Maier, N. J. Halas, P. Nordlander, H. Giessen, and C. T. Chong, The Fano Resonance in Plasmonic Nanostructures and Metamaterials, *Nat. Mater.* **9**, 707 (2010).
- [41] S. N. Sheikholeslami, A. García-Etxarri, and J. A. Dionne, Controlling the Interplay of Electric and Magnetic Modes via Fano-like Plasmon Resonances, *Nano Lett.* **11**, 3927 (2011).
- [42] N. Liu, S. Mukherjee, K. Bao, Y. Li, L. V. Brown, P. Nordlander, and N. J. Halas, Manipulating Magnetic Plasmon Propagation in Metallic Nanocluster Networks, *ACS Nano* **6**, 5482 (2012).
- [43] S. Campione, C. Guclu, R. Ragan, and F. Capolino, Enhanced Magnetic and Electric Fields via Fano Resonances in Metasurfaces of Circular Clusters of Plasmonic Nanoparticles, *ACS Photonics* **1**, 254 (2014).
- [44] C. Guclu, M. Veysi, M. Darvishzadeh-Varcheie, and F. Capolino, Artificial Magnetism via Nanoantennas under Azimuthally Polarized Vector Beam Illumination, in *Conference on Lasers and Electro-Optics, OSA Technical Digest (Optical Society of America, 2016)*, paper JW2A.21.
- [45] C. Guclu, M. Veysi, M. Darvishzadeh-Vercheie, and F. Capolino, Optical Nanoantennas as Magnetic Nanoprobes for Enhancing Light-Matter Interaction, in *2016 10th Int. Congr. Adv. Electromagn. Mater. Microw. Opt. METAMATERIALS (2016)*, pp. 391–393.
- [46] F. Shafiei, F. Monticone, K. Q. Le, X.-X. Liu, T. Hartsfield, A. Alù, and X. Li, A Subwavelength Plasmonic Metamolecule Exhibiting Magnetic-Based Optical Fano Resonance, *Nat. Nanotechnol.* **8**, 95 (2013).
- [47] A. E. Krasnok, A. E. Miroshnichenko, P. A. Belov, and Y. S. Kivshar, All-Dielectric Optical Nanoantennas, *Opt. Express* **20**, 20599 (2012).
- [48] R. Hussain, S. S. Kruk, C. E. Bonner, M. A. Noginov, I. Staude, Y. S. Kivshar, N. Noginova, and D. N. Neshev, Enhancing Eu³⁺ Magnetic Dipole Emission by Resonant Plasmonic Nanostructures, *Opt. Lett.* **40**, 1659 (2015).
- [49] C. Guclu, M. Veysi, and F. Capolino, Photoinduced Magnetic Nanoprobe Excited by an Azimuthally

- Polarized Vector Beam, *ACS Photonics* **3**, 2049 (2016).
- [50] A. I. Kuznetsov, A. E. Miroschnichenko, M. L. Brongersma, Y. S. Kivshar, and B. Luk'yanchuk, Optically Resonant Dielectric Nanostructures, *Science* **354**, aag2472 (2016).
- [51] R. Wilson, The Use of Gold Nanoparticles in Diagnostics and Detection, *Chem. Soc. Rev.* **37**, 2028 (2008).
- [52] G. L. Nealon, B. Donnio, R. Greget, J.-P. Kappler, E. Terazzi, and J.-L. Gallani, Magnetism in Gold Nanoparticles, *Nanoscale* **4**, 5244 (2012).
- [53] G. Peng, U. Tisch, O. Adams, M. Hakim, N. Shehata, Y. Y. Broza, S. Billan, R. Abdah-Bortnyak, A. Kuten, and H. Haick, Diagnosing Lung Cancer in Exhaled Breath Using Gold Nanoparticles, *Nat. Nanotechnol.* **4**, 669 (2009).
- [54] S. Zeng, K.-T. Yong, I. Roy, X.-Q. Dinh, X. Yu, and F. Luan, A Review on Functionalized Gold Nanoparticles for Biosensing Applications, *Plasmonics* **6**, 491 (2011).
- [55] D. Liu, Z. Wang, and X. Jiang, Gold Nanoparticles for the Colorimetric and Fluorescent Detection of Ions and Small Organic Molecules, *Nanoscale* **3**, 1421 (2011).
- [56] C. Wu, A. B. Khanikaev, R. Adato, N. Arju, A. A. Yanik, H. Altug, and G. Shvets, Fano-Resonant Asymmetric Metamaterials for Ultrasensitive Spectroscopy and Identification of Molecular Monolayers, *Nat. Mater.* **11**, 69 (2012).
- [57] Z. Zhang, R. D. Ross, and R. K. Roeder, Preparation of Functionalized Gold Nanoparticles as a Targeted X-Ray Contrast Agent for Damaged Bone Tissue, *Nanoscale* **2**, 582 (2010).
- [58] M. Veysi, C. Guclu, and F. Capolino, Vortex Beams with Strong Longitudinally Polarized Magnetic Field and Their Generation by Using Metasurfaces, *J. Opt. Soc. Am. B* **32**, 345 (2015).
- [59] M. Veysi, C. Guclu, and F. Capolino, Focused Azimuthally Polarized Vector Beam and Spatial Magnetic Resolution below the Diffraction Limit, *JOSA B* **33**, 2265 (2016).
- [60] S. Steshenko and F. Capolino, in *Theory Phenom. Metamaterials* (CRC Press, 2009).
- [61] S. Campione, S. M. Adams, R. Ragan, and F. Capolino, Comparison of Electric Field Enhancements: Linear and Triangular Oligomers versus Hexagonal Arrays of Plasmonic Nanospheres, *Opt. Express* **21**, 7957 (2013).
- [62] N. J. H. N. K. Grady, Grady, N. K., Halas, N. J. & Nordlander, P. Influence of Dielectric Function Properties on the Optical Response of Plasmon Resonant Metallic Nanoparticles. *Chem. Phys. Lett.* **399**, 167-171, *Chem. Phys. Lett.* **399**, 167 (2004).
- [63] J. D. Jackson, *Classical Electrodynamics*, 3rd ed. (Wiley, 1998).
- [64] A. Vallecchi, S. Campione, and F. Capolino, Symmetric and Antisymmetric Resonances in a Pair of Metal-Dielectric Nanoshells: Tunability and Closed-Form Formulas, *J. Nanophotonics* **4**, 041577 (2010).
- [65] A. Vallecchi and F. Capolino, in *Theory Phenom. Metamaterials* (CRC Press, 2009).
- [66] L. Li and C.-H. Liang, ANALYSIS OF RESONANCE AND QUALITY FACTOR OF ANTENNA AND SCATTERING SYSTEMS USING COMPLEX FREQUENCY METHOD COMBINED WITH MODEL-BASED PARAMETER ESTIMATION, *Prog. Electromagn. Res.* **46**, 165 (2004).
- [67] R. Carminati, J.-J. Greffet, C. Henkel, and J. M. Vigoureux, Radiative and Non-Radiative Decay of a Single Molecule close to a Metallic Nanoparticle, *Opt. Commun.* **261**, 368 (2006).
- [68] L. Novotny and B. Hecht, *Principles of Nano-Optics*, 2nd ed. (Cambridge University Press, 2012).
- [69] I. Liberal, Y. Ra'di, R. Gonzalo, I. Ederra, S. A. Tretyakov, and R. W. Ziolkowski, Least Upper Bounds of the Powers Extracted and Scattered by Bi-Anisotropic Particles, *IEEE Trans. Antennas Propag.* **62**, 4726 (2014).
- [70] I. Liberal, I. Ederra, R. Gonzalo, and R. W. Ziolkowski, Upper Bounds on Scattering Processes and Metamaterial-Inspired Structures That Reach Them, *IEEE Trans. Antennas Propag.* **62**, 6344 (2014).